*J. Fluid Mech.* (2011), *vol.* 670, *pp.* 204–213. 
doi:10.1017/S0022112010006294

# Variations on Kolmogorov flow: turbulent energy dissipation and mean flow profiles

B. ROLLIN[1]†, Y. DUBIEF[2] AND C.R. DOERING[3]

[1]Los Alamos National Laboratory, Los Alamos, NM 87544, USA

[2]School of Engineering, University of Vermont, Burlington, VT 05405, USA

[3]Department of Mathematics, Department of Physics and Center for the Study of Complex Systems, University of Michigan, Ann Arbor, MI 48109-1107, USA

(Received 21 May 2010; revised 19 November 2010; accepted 4 December 2010)

The relation between the form of a body force driving a turbulent shear flow and the dissipation factor $\beta = \varepsilon\ell/U^3$ is investigated by means of rigorous upper bound analysis and direct numerical simulation. We consider unidirectional steady forcing functions in a three-dimensional periodic domain and observe that a rigorous infinite Reynolds number bound on $\beta$ displays the same qualitative behaviour as the computationally measured dissipation factor at finite Reynolds number as the force profile is varied. We also compare the measured mean flow profiles with the Stokes flow profile for the same forcing. The mean and Stokes flow profiles are strikingly similar at the Reynolds numbers obtained in the numerical simulations, lending quantitative credence to the notion of a turbulent eddy viscosity.

**Key words:** Navier–Stokes equations, turbulence modelling, variational methods

## 1. Introduction

In the first half of the last century, Richardson (1922), Taylor (1938) and Kolmogorov (1941) developed a theory of turbulence based on the concept of a cascade whereby energy is transferred at a constant rate from larger unstable eddies to smaller eddies until viscosity effectively dissipates the kinetic energy. For incompressible Newtonian fluids, the energy dissipation rate per unit mass is

$$\varepsilon = 2\nu\langle S_{ij}S_{ij}\rangle, \tag{1.1}$$

where $S_{ij}$ is the rate of strain tensor, $\nu$ is the kinematic viscosity coefficient, and $\langle\cdot\rangle$ is an appropriate averaging procedure. The 'zeroth law of turbulence' asserts that, all other controls held constant, $\varepsilon$ tends to a finite positive limit as $\nu \to 0$ (Sreenivasan 1984; Frisch 1995). Specifically, suppose $U = \langle \boldsymbol{u}^2\rangle^{1/2}$ is the steady-state root mean square (r.m.s.) velocity in a statistical steady state where $\langle\cdot\rangle$ is a space–time average, $\ell$ is a characteristic length scale, the Reynolds number is

$$Re = U\ell/\nu, \tag{1.2}$$

and the dimensionless dissipation factor is defined by

$$\beta = \varepsilon\ell/U^3. \tag{1.3}$$

† Email address for correspondence: bertrand@lanl.gov

The zeroth law may then be interpreted as the claim that for developed turbulence, $\beta(Re) \to \beta(\infty) > 0$ as $Re \to \infty$. This leaves us with the issue of the theoretical prediction of the magnitude of the residual energy dissipation $\beta(\infty)$ and its dependence on details of the forces driving the flow (Sreenivasan 1998). These questions are the central focus of this paper.

An analysis of the Navier–Stokes equations has produced rigorous limits on the mean energy dissipation rate for incompressible flows directly from the governing Navier–Stokes equations without additional hypothesis or approximations. Physically relevant results for some boundary driven flows were first derived in the 1960s by Howard (1972) and Busse (1978) and developed and extended further several decades later (Doering & Constantin 1992, 1994; Wang 1997; Kerswell 1998). Rigorous limits on bulk dissipation for body-force-driven flows in a fully periodic domain have been developed by Foias, Manley & Temam (1993), Foias (1997), Childress, Kerswell & Gilbert (2001) and Doering & Foias (2002). The last named work showed that for general square-integrable steady body forces, the energy dissipation rate is bounded from above according to

$$\varepsilon \leqslant c_1 \nu U^2/\ell^2 + c_2 U^3/\ell, \tag{1.4}$$

where, specifically, $\ell$ is the longest characteristic length scale in the body-force function and the finite positive coefficients $c_1$ and $c_2$ depend only on the functional 'shape' (defined precisely in the next section) of the body force. Dividing by $U^3/\ell$ yields

$$\beta(Re) \leqslant c_1 \frac{1}{Re} + c_2, \tag{1.5}$$

in qualitative agreement with theoretical, computational and experimental results for homogeneous isotropic turbulence. (This form of an upper bound for $\beta(Re)$ depends crucially on the square-integrability of the forcing function. 'Fractal' body forces with significant components at small length scales may produce high-Reynolds-number dissipation factors and estimates $\beta(Re) \lesssim Re^{\alpha}$, with exponent $\alpha > 0$ that depends on details of the high-wavenumber spectrum of the forcing; see Cheskidov, Doering & Petrov (2007).) Soon thereafter, Doering, Eckhardt & Schumacher (2003) derived an explicit upper bound for $\beta(\infty)$ depending only on the shape of a unidirectional driving force in a channel with stress-free walls; see also Petrov, Lu & Doering (2005).

In this paper, we describe a study of qualitative features of the high-Reynolds-number dissipation factor by considering variations of Kolmogorov forcing, i.e. steady unidirectional body forces of varying profiles, both by upper bound theory and via direct numerical simulations (DNS). This study aims at showing that the upper bound theory, valid when $Re \to \infty$, gives an indication of $\beta$ at large but finite $Re$. Turbulence driven by Kolmogorov forces with monochromatic (single wavenumber) profiles has previously been studied in DNS by Borue & Orszag (1996) and also via an upper bound analysis by Childress *et al.* (2001), but this is the first attempt to systematically investigate the force-shape dependence of some aspects of the turbulence. The remainder of the paper is organized as follows. In the next section, we describe the upper bound analysis for steady generalized Kolmogorov forces in a periodic domain. In § 3, we investigate the force-shape dependence of the asymptotic high-Reynolds-number bound on the dissipation factor, and in § 4 we compare the rigorous estimates with the DNS results. In § 5, we compare the observed mean flow profiles with Stokes flow profiles, which for these Kolmogorov forces are also steady Navier–Stokes solutions, albeit with an appropriately renormalized eddy viscosity. Section 6 contains a brief summary and discussion of the results.

## 2. Bound on the dissipation factor

Consider a body-force-driven incompressible flow on a three-dimensional periodic domain of volume $L_x \times L_y \times L_z$. The dynamics is governed by the Navier–Stokes equations

$$\frac{\partial \boldsymbol{u}}{\partial t} + (\boldsymbol{u} \cdot \nabla)\boldsymbol{u} + \nabla p = \nu \nabla^2 \boldsymbol{u} + \boldsymbol{f}, \tag{2.1}$$

$$\nabla \cdot \boldsymbol{u} = 0, \tag{2.2}$$

where $\boldsymbol{u}(\boldsymbol{x}, t)$ is the velocity vector field, $p(\boldsymbol{x}, t)$ is the pressure, and $\boldsymbol{f}(\boldsymbol{x})$ is a steady driving force. A recent estimate of an upper bound on the dissipation factor $\beta$ can be found in Dascaliuc, Foias & Jolly (2009). However, Doering *et al.* (2003) provide an upper bound on $\beta$ that explicitly and only depends on the shape of the forcing function for a channel flow. Here, we generalize that estimate to the case of a three-dimensional domain with fully periodic boundary conditions. In the following, we limit ourselves to recalling key points of the derivation, highlighting the differences, and refer to the earlier work for detailed descriptions of the parts of the analysis that are the same.

The steady generalized Kolmogorov force driving the flow is

$$\boldsymbol{f}(\boldsymbol{x}) = F\phi(y/l)\boldsymbol{e}_x, \tag{2.3}$$

where $l$, an integer fraction of $L_y$, is the longest length scale in the forcing profile, $F$ is the forcing amplitude, and the dimensionless square integrable (or smoother) shape function $\phi(\eta)$ satisfies periodic boundary conditions for $\eta \in [0, 1]$ with zero mean, $\int_0^1 \phi(\eta)\,\mathrm{d}\eta = 0$. When the shape function is normalized, for example by $\int_0^1 \phi(\eta)^2\,\mathrm{d}\eta = 1$, then a unique forcing amplitude $F$ is defined.

We introduce the dimensionless 'potential' $\Phi(\eta)$, also periodic on [0,1], defined up to an additive constant by $\Phi' = -\phi$. Next, we introduce another periodic (on [0,1]) mean-zero 'multiplier' function $\psi(\eta)$ that is not orthogonal to $\phi$, i.e. $\int_0^1 \phi(\eta)\psi(\eta)\,\mathrm{d}\eta \neq 0$, and define the derivative of the multiplier function $\Psi(\eta) = \psi'(\eta)$, which is also periodic and zero mean. The inner product of $\phi$ and $\psi$ is equal to the inner product of $\Phi$ and $\Psi$: $\int_0^1 \Phi(\eta)\Psi(\eta)\,\mathrm{d}\eta = \int_0^1 \phi(\eta)\psi(\eta)\,\mathrm{d}\eta$.

For a statistically steady flow such as developed turbulence, Doering *et al.* (2003) showed that a formulation for $\beta$ using the potential $\Phi$ and derivative multiplier $\Psi$ is

$$\beta = \frac{\langle \Phi' u \rangle \langle \Psi u v + Re^{-1}\Psi' u \rangle}{\langle \Phi \Psi \rangle}, \tag{2.4}$$

where $u$ and $v$ are the streamwise and vertical components of the velocity field scaled by the r.m.s. speed $U$. The upper bound $\beta_b$ on the dissipation factor is obtained by maximizing the right-hand side of (2.4) over all such unit normalized, periodic, divergence-free velocity fields and then minimizing over all appropriate multiplier functions $\Psi$:

$$\beta \leqslant \min_{\Psi} \max_{\mathbf{u}} \left[ \frac{\langle \Phi' u \rangle \langle \Psi u v \rangle}{\langle \Phi \Psi \rangle} + Re^{-1} \frac{\langle \Phi' u \rangle \langle \Psi' u \rangle}{\langle \Phi \Psi \rangle} \right] = \beta_b(Re). \tag{2.5}$$

Note that the maximization is over a set of velocity fields that is larger than, but includes, the solution set of the Navier–Stokes equation. The bound $\beta_b$ depends on the Reynolds number (which we display explicitly) and the shape of the applied force $\phi = -\Phi'$.

Focusing on the $Re \to \infty$ limit, Doering *et al.* (2003) showed that

$$\limsup_{Re\to\infty} \beta(Re) \leqslant \beta_b(\infty) = \min_{\Psi} \frac{1}{\sqrt{27}} \frac{\langle \phi^2 \rangle^{1/2}}{\langle \Phi\Psi \rangle} \sup_{y\in[0,1]} |\Psi(y)|, \tag{2.6}$$

and evaluating this minimum over multiplier functions $\Psi(y)$ is where the difference with Doering *et al.* (2003) appears. Given periodic mean-zero functions $\Phi(y)$ and $\Psi(y)$, for any constant $C$,

$$\int_0^1 \Phi(y')\,\Psi(y')\,\mathrm{d}y' = \int_0^1 [\Phi(y') - C]\,\Psi(y')\,\mathrm{d}y' \leqslant \int_0^1 |\Phi(y') - C|\,\mathrm{d}y' \times \sup_y |\Psi(y)|. \tag{2.7}$$

Inequality (2.7) is saturated by functions $\Psi_m(y) \sim \mathrm{sign}[\Phi(y) - C]$. Thus,

$$\beta_b(\infty) = \frac{1}{\sqrt{27}} \frac{\langle \phi^2 \rangle^{1/2}}{\min_C \int_0^1 |\Phi(y') - C|\,\mathrm{d}y'}. \tag{2.8}$$

To determine the critical value $C_m$ realizing the extremum, we regularize the denominator of (2.8) by writing

$$\begin{aligned} \min_C \int_0^1 |\Phi(y) - C|\,\mathrm{d}y &= \min_C \lim_{\delta\to 0} \int_0^1 \sqrt{(\Phi(y) - C)^2 + \delta^2}\,\mathrm{d}y \\ &= \lim_{\delta\to 0} \min_C \int_0^1 \sqrt{(\Phi(y) - C)^2 + \delta^2}\,\mathrm{d}y. \end{aligned} \tag{2.9}$$

Then, the condition defining $C_m$ is

$$0 = \frac{\mathrm{d}}{\mathrm{d}C} \int_0^1 \sqrt{(\Phi(y) - C)^2 + \delta^2}\,\mathrm{d}y \bigg|_{C=C_m} = \int_0^1 \frac{\Phi(y) - C_m}{\sqrt{(\Phi(y) - C_m)^2 + \delta^2}}\,\mathrm{d}y \tag{2.10}$$

and sending $\delta \to 0$ we conclude that

$$0 = \int_0^1 \mathrm{sign}[\Phi(y') - C_m]\,\mathrm{d}y'. \tag{2.11}$$

This uniquely fixes $C_m$ and thus

$$\beta_b(\infty) = \frac{1}{\sqrt{27}} \frac{\sqrt{\langle \phi^2 \rangle}}{\langle |\Phi - C_m| \rangle}. \tag{2.12}$$

## 3. Force-shape dependence of the dissipation factor

The body-force shape dependence of the dissipation factor is investigated on a family of generalizations of the traditional Kolmogorov forcing $\sim \boldsymbol{e}_x \sin 2\pi y/L_y$ by adding a second component with amplitude $A_k$ for an additional integer wavenumber $k$:

$$\boldsymbol{f}(\boldsymbol{x}) = [\sin(2\pi y/L_y) + A_k \sin(2\pi k y/L_y)]\boldsymbol{e}_x \quad \text{for} \quad k \geqslant 2. \tag{3.1}$$

Then, the amplitude and normalized shape functions are respectively

$$F = \sqrt{\frac{1 + A_k^2}{2}}, \qquad \phi(\eta) = \sqrt{\frac{2}{1 + A_k^2}}\ [\sin(2\pi\eta) + A_k \sin(2\pi k\eta)]. \tag{3.2}$$

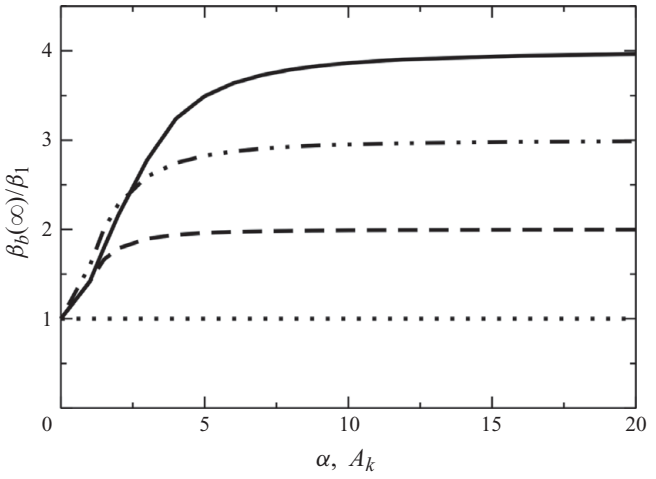


FIGURE 1. High-Reynolds-number dissipation factor $\beta_b(\infty)$ from (3.3), normalized by $\beta_1 \equiv \beta_b(\infty)$ for the traditional Kolmogorov force (i.e. $\pi^2/\sqrt{54}$), plotted as a function of the amplitude of the second mode forced, $A_k$ (or amplitude $\alpha$ for classic Kolmogorov force). Dotted line, simple Kolmogorov force $\boldsymbol{f}(\boldsymbol{x}) = \alpha \sin(2\pi y/l)\boldsymbol{e}_x$; dashed line, $\boldsymbol{f}(\boldsymbol{x}) = [\sin(2\pi y/l) + A_2 \sin(2 \times 2\pi y/l)]\,\boldsymbol{e}_x$; dash-dotted line, $\boldsymbol{f}(\boldsymbol{x}) = [\sin(2\pi y/l) + A_3 \sin(3 \times 2\pi y/l)]\,\boldsymbol{e}_x$; solid line, $\boldsymbol{f}(\boldsymbol{x}) = [\sin(2\pi y/l) + A_4 \sin(4 \times 2\pi y/l)]\,\boldsymbol{e}_x$.

We use (2.12) to evaluate the high-$Re$ bound on $\beta$ for these shapes:

$$\beta_b(\infty) = \frac{1}{\sqrt{27}} \frac{1}{\displaystyle\int_0^1 \left| \frac{1}{2\pi}\sqrt{\frac{2}{1+A_k^2}} \left( \cos(2\pi\eta) + \frac{A_k}{k}\cos(2\pi k\eta) \right) - C_m \right| \mathrm{d}\eta}. \tag{3.3}$$

The integrals in the denominator of (3.3) can be easily evaluated numerically, but first we consider some simple cases. The case of the classical Kolmogorov forcing ($A_k = 0$ and $C_m = 0$) is straightforward:

$$\beta_b(\infty) = \frac{1}{\sqrt{27}} \frac{1}{\displaystyle\int_0^1 \left| \frac{1}{2\pi}\sqrt{2}\cos(2\pi\eta) \right| \mathrm{d}\eta} = \frac{\pi^2}{\sqrt{54}} = 1.343\ldots \equiv \beta_1. \tag{3.4}$$

Another elementary case is when $A_k \gg 1$ and the contribution of the primary term to the forcing function can be neglected. Then, the driving is a Kolmogorov force with fundamental wavenumber greater than the minimum wavenumber and

$$\beta_b(\infty) = \frac{1}{\sqrt{27}} \frac{1}{\dfrac{1}{2\pi}\sqrt{\dfrac{2}{A_k^2}} \displaystyle\int_0^1 \left| \frac{A_k}{k}\cos(2\pi k\eta) \right| \mathrm{d}\eta} = \frac{k\pi^2}{\sqrt{54}}. \tag{3.5}$$

Hence, when the longest scale in the force profile $\ell$ is used in the definition $\beta = \varepsilon\ell/U^3$, the upper bound on the asymptotic high-$Re$ value of the dissipation factor is linearly proportional to $k = L/\ell$.

Figure 1 shows the bound on $\beta_b(\infty)$ from (3.3) for a non-trivial force-shape normalized by the value of $\beta_b(\infty)$ obtained for the classic Kolmogorov force, i.e. $\pi^2/\sqrt{54}$, as a function of the amplitude of the secondary term. In addition to the

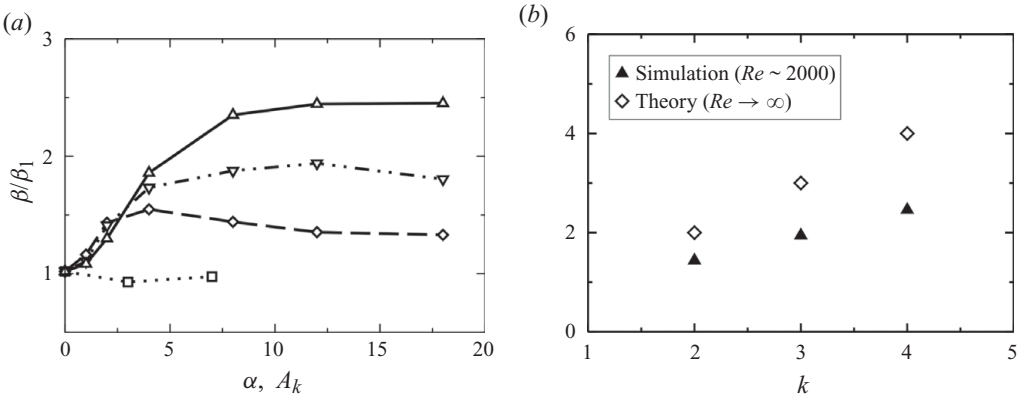


FIGURE 2. Ratio between the measured dissipation factor $\beta$ for a given force shape and the asymptotic dissipation factor for the Kolmogorov force shape $\beta_1$. (*a*) $\beta/\beta_1$ from DNS as a function of the larger mode amplitude, $A_k$ (or amplitude $\alpha$ for the classic Kolmogorov force shape). $\beta_1$ is the average value of $\beta$ in simulations using a Kolmogorov forcing, since these simulations appear to be in the asymptotic regime for $\beta$. Squares, dotted line, $\boldsymbol{f}(\boldsymbol{x}) = \alpha \sin(2\pi y/l)\,\boldsymbol{e}_x$, $\alpha = 1, 3, 7$; otherwise, $\boldsymbol{f}(\boldsymbol{x}) = [\sin(2\pi y/l) + A_k \sin(k \times 2\pi y/l)]\,\boldsymbol{e}_x$; diamonds, dashed line, $k = 2$; down triangles, dash-dotted line, $k = 3$; up triangle, solid line, $k = 4$. (*b*) $\beta/\beta_1$ as a function of the larger mode forced, at constant Reynolds number ($Re \sim 2000$). Here $\beta_1$ is defined as previously for the DNS data and takes the theoretical value otherwise. Solid symbols are DNS results for $A_2 = 8$, $A_3 = 12$ and $A_4 = 18$. For these amplitudes, the computed dissipation factors are presumably close to their asymptotic values (see figure 2*a*). Hollow symbols are asymptotic predictions by theory (see (3.4) and (3.5)).

property exposed by (3.5), this figure also shows that $\beta_b(\infty)$ is quite sensitive to the change in shape of the forcing function. Indeed, $\beta_b(\infty)$ increases as soon as a secondary term is added to the original Kolmogorov forcing, and then eventually plateaus when the higher wavenumber term becomes dominant.

## 4. Comparison with direct numerical simulations

DNS were performed using a fully de-aliased spectral code. The time stepping was based on a third-order Runge–Kutta algorithm for the nonlinear and forcing terms, the viscous term was integrated through an analytic factor, and stability was ensured by a Courant–Friedrichs–Lewy (CFL) condition. The flow was computed in a $2\pi$ periodic cubic box with $128 \times 128 \times 128$ grid points. The viscosity was set to $\nu = 0.015625$, large enough to ensure satisfactory resolution of the turbulence.

While the bounds on the dissipation factor, $\beta$, are derived in the infinite Reynolds number limit, we compare them with finite Reynolds number DNS. Considering the computer power available nowadays, we can only hope that Reynolds numbers of DNS are high enough, so that the variables considered display some of their features as in the infinite Reynolds number limit. Figure 2(*a*) shows the measured dissipation factors $\beta$ normalized by the average value of $\beta$ in the case of the classic Kolmogorov forcing at different amplitudes as a function of the amplitude of the secondary term. The symbols designating a particular secondary wavenumber $k$ are linked by straight lines using the same nomenclature as in figure 1 to facilitate comparison between the infinite Reynolds number bounds there, and the results of the finite Reynolds number simulations where the Taylor microscale Reynolds number, $R_\lambda$, varies between about 50 and 100. We verified that all the simulations

satisfied the convergence criterion for the Kolmogorov flow defined by Sarris *et al.* (2007). The simulations with secondary term amplitudes of $A_k = 18$ satisfied $k_{max}\lambda_K > 1.2$, where $k_{max}$ was the largest wavenumber of the simulation and $\lambda_K$ the Kolmogorov length scale, slightly under the commonly used flow resolution criterion $k_{max}\lambda_K > 1.5$.

The central point is the qualitative similarity of figures 1 and 2($a$). Firstly, $\beta$ has a nearly constant value when only one mode is forced, suggesting that the turbulence is reasonably well developed at these parameter values to be in the asymptotic regime for $\beta$. (In the case of the traditional Kolmogorov forcing, the limit of resolution was achieved for amplitude $\alpha = 7$.) Secondly, for the multi-mode force shapes, $\beta$ increases as a function of $A_k$ until the secondary term becomes dominant and $\beta$ plateaus, reaching its asymptotic value. A slight decrease in the dissipation factor is observed for $k = 2$ and $k = 3$ as $A_k$ increases. A possible cause for this slight overshoot might be a comparable contribution of the modes in the forcing function. As in figure 2($a$), figure 2($b$) shows the dissipation factor enhancement, $\beta/\beta_1$, but at a constant Reynolds number ($Re \sim 2000$), as a function of the secondary mode in the forcing function. We observe that the analytical upper bound estimate on the dissipation factor predicts qualitatively the linear pattern of the dissipation factor at a modest and constant Reynolds number. The quantitative mismatch may be due to some viscous effects or to the upper bound estimate. Much higher-resolution simulations are needed to address this issue, and will be left for future work. Patterns observed in figures 2($a$) and 2($b$) are indications that, in this study, the constraint is to be in a sufficiently turbulent regime (Reynolds number high but not necessarily constant) to observe the qualitative behaviour extracted from the analysis.

The analytic upper bound on the dissipation factor in the infinite Reynolds number limit thus qualitatively predicts the behaviour of $\beta$ in the relatively low-Reynolds-number turbulent simulations. The dissipation factor is not only sensitive to the shape of the forcing but also depends strongly on it.

Despite the qualitative agreement of figures 1 and 2, the numerical values for $\beta$ are about a factor 5 below the upper bound (Doering *et al.* 2003), not visible here because of the normalization of $\beta$ in the figures. Figures 1 and 2($a$) also clearly show that the bounds do not accurately predict the magnitude of the increase in $\beta$ when the force includes an additional wavenumber. The increase, i.e. the sensitivity to the details of the force shape, are larger in the infinite Reynolds number upper bounds than observed in the simulations. Nevertheless, it is interesting to note that upper bound analysis can predict some features of the force-shape dependence.

## 5. Mean velocity profile dependence on the force profile

Figure 3 shows the measured mean velocity profiles $U(y)$, the profile shape $U_{Stokes}(y)$ of the associated Stokes flow, the infinite Reynolds number optimal multiplier profile $\psi_m(y)$ and the corresponding forcing function $f(y) = \sin(y) + \sin(ky)$, where $k = 2, 3, 4$ respectively in figures 3($a$), 3($b$) and 3($c$). The steady Stokes flow solving $0 = \tilde{\nu}U''_{Stokes}(y) + F\phi(y/l)$ (which for these Kolmogorov-like forces is also a solution of Navier–Stokes) realizes the lower bound on the dissipation factor $\beta$ given the mean power balance; its profile shape is simply obtained by integrating the forcing function twice:

$$U_{Stokes}(y) = -\frac{F}{\tilde{\nu}} \int_0^y \left( \int_0^{y'} F\phi(y''/l)\, \mathrm{d}y'' \right) \mathrm{d}y'. \tag{5.1}$$

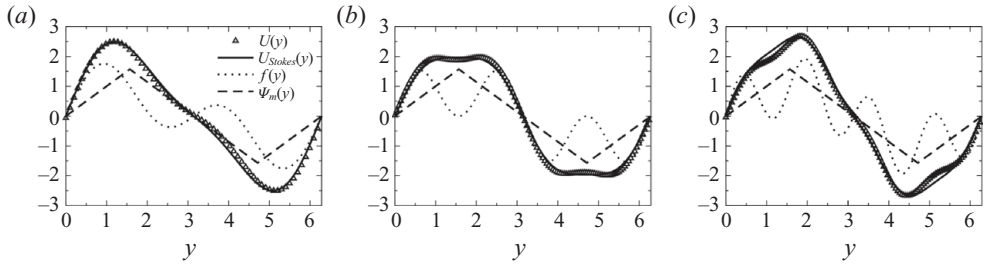


FIGURE 3. Mean velocity profile $U(y)$ (triangles), rescaled Stokes flow profile $U_{Stokes}(y)$ (solid line), optimal multiplier profile $\psi_m(y)$ (piecewise linear dashed line) and corresponding forcing profiles $f(y)$ (dotted line). (*a*) $f(y) = \sin(y) + \sin(2y)$, (*b*) $f(y) = \sin(y) + \sin(3y)$ and (*c*) $f(y) = \sin(y) + \sin(4y)$.

The Stokes profiles plotted in figure 3 have in each case been rescaled, by adjusting the effective viscosity $\tilde{\nu}$, for plotting along with the data. The infinite Reynolds number optimal multiplier $\psi_m$ is defined by (the normalization is arbitrary)

$$\psi_m(y) = \int_0^y \operatorname{sign}\left(\int_0^{y'} \phi(y''/l)\,\mathrm{d}y'' - C\right)\mathrm{d}y', \tag{5.2}$$

where $C$ is the parameter determined by the zero-mean condition.

A key feature of the observed mean velocity profiles is that they are strikingly similar to the Stokes flow profiles. For the mean velocity profiles shown in figure 3, the dominant mode is clearly the basic sine function but the relative amplitude of the secondary term is properly reflected in the Stokes flow profiles. However, the magnitude of the Stokes flow in (5.1) using the molecular viscosity $\nu$ is much larger than the measured mean flow. The rescaling employed in the plots amounts to the utilization of a renormalized turbulent eddy-viscosity value for $\tilde{\nu}$. In their simulations with a single-mode Kolmogorov force, Borue & Orszag (1996) noted the validity of the concept of an effective viscosity in the sense that the mean flow profiles were also simple sinusoids, albeit with an appropriately suppressed amplitude. In the results presented here, the eddy-viscosity concept is put to – and passes – a more stringent test: the relative contributions of the modes in the generalized Kolmogorov forces to the mean profile are in quantitative accord with the standard diffusive suppression of higher wavenumbers. Distinct from the DNS presented in Doering *et al.* (2003), where the flow was bounded by channel walls and the mean flow profile appeared linear despite a single Fourier mode forcing, the domain used for the simulations here is periodic in all three directions without any (even free-slip) boundaries to constrain turbulent velocity fluctuations. This apparently allows the turbulence to generate an effective diffusion of momentum that is well described, at least on relatively long length scales, by an effective viscosity coefficient. A detailed investigation of effective eddy viscosity for these flows is being pursued in a modelling perspective, and we shall report the findings in a future publication.

The optimal multiplier profiles in figure 3 reflect only the primary term of the forcing functions; they are clearly sensitive to different features of the forcing than the mean flow profile. Figure 4 allows a broader perspective on behaviour of the optimal multiplier $\psi_m$. In this figure, we plot the optimal multiplier profile, the mean velocity profile and the normalized force profile as the amplitude of the secondary mode is increased. We observe that $\psi_m$ can be less sensitive to the force shape

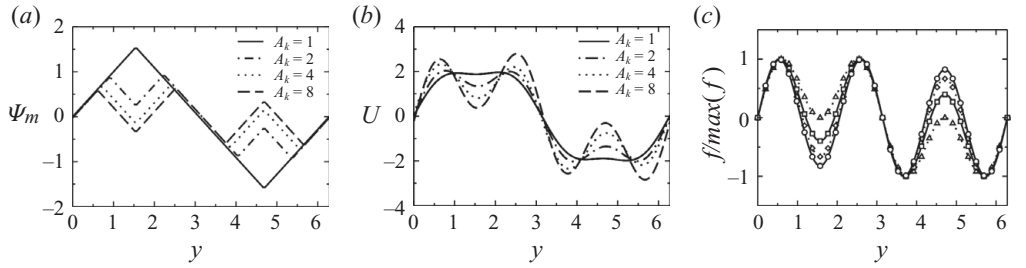


FIGURE 4. (*a*) Optimal multiplier profiles $\psi_m(y)$ for the force profiles $\sin(y) + A_k \sin(3y)$ for $A_k = 1, 2, 4, 8$. (*b*) Mean velocity profiles $U(y)$ for the force profiles $\sin(y) + A_k \sin(3y)$ for $A_k = 1, 2, 4, 8$. (*c*) Force profiles $\sin(y) + A_k \sin(3y)$ for $A_k = 1, 2, 4, 8$, normalized by their maximum values. Triangles on dotted line, $A_k = 1$; squares on solid line, $A_k = 2$; diamonds on dotted line, $A_k = 4$; circles on solid line, $A_k = 8$.

than the mean flow profile. Indeed, $\psi_m$ displays the same profile for force shapes $\sin(y)$ and $\sin(y) + \sin(3y)$. For larger amplitudes ($A_k \geqslant 2$), $\psi_m$ displays a shape characteristic of the wavenumbers composing the force shape. Figure 4(*b*) also shows that the relation between $\psi_m$ and the mean velocity profile is unclear. For the force shape $\sin(y) + \sin(3y)$, for example, the optimal multiplier shows no indication of the influence of the secondary term whereas the mean velocity profile clearly does.

## 6. Conclusions

The influence of the shape of a driving body force on the bulk energy dissipation rate $\beta = \varepsilon \ell / U^3$ was investigated by means of rigorous analysis and DNS. Upper bounds on the asymptotic high-Reynolds-number dissipation factor, depending explicitly on the form of generalized Kolmogorov-like forcing functions in a domain without boundaries, were derived by variational methods. Then, simulations at finite Reynolds numbers in a fully periodic domain confirmed qualitative predictions of the mathematical analysis at infinite Reynolds numbers. These results confirm the dependence of the dissipation factor on the force shape, as anticipated by the solution of the optimization problem for the best bound. We discern two major tendencies: (i) when the forcing function is mainly shaped by a single wavenumber, the high-Reynolds-number dissipation factor is approximately proportional to the dominant wavenumber, and (ii) $\beta$ increases as additional higher wavenumber components on increasing amplitude are added to the forcing function.

We also observed that the measured mean velocity profiles were very well described by a Stokes-like profile utilizing an effective eddy viscosity, providing quantitative validation of the concept, at least for the restricted class of turbulent flows considered here. The optimal multiplier function employed in the derivation of the variational bounds is also related to the force shape, but in a highly nonlinear way; its relation to the mean velocity profile – and its physical significance, if there is any – remains unclear.

In this paper, we have demonstrated that in unbounded turbulence the shape of the forcing plays a major role in the energy dissipation rate. The variational upper bound approach adapted from the analysis of Doering *et al.* (2003) captures this dependence qualitatively for a variety of generalized turbulent Kolmogorov flows and the high-Reynolds-number predictions from the analysis remain qualitatively valid for even moderate Reynolds numbers. Improvements in the quantitative prediction of

the dissipation factor would be necessary in order to be able to use such a theoretical dissipation in a turbulence model, but the successful theoretical prediction of some features of the turbulence bodes well for the role that rigorous mathematical analysis may play in the study of developed turbulent flows.

This work was supported in part by NSF Awards PHY-0555324 and PHY-0855335. Computational resources provided by the Vermont Advanced Computing Center, supported by NASA (grant NNX 06AC88G), are gratefully acknowledged. We are also grateful to Professors D. Carati and B. Knaepen and all the Turbo team for providing the simulation code.

## REFERENCES

Borue, V. & Orszag, S. A. 1996 Numerical study of three-dimensional Kolmogorov flow at high Reynolds numbers. *J. Fluid Mech.* **306**, 293–323.

Busse, F. H. 1978 The optimum theory of turbulence. *Adv. Appl. Mech.* **18**, 77–121.

Cheskidov, A., Doering, C. R. & Petrov, N. P. 2007 Energy dissipation in fractal-forced flow. *J. Math. Phys.* **48**, 065208.

Childress, S., Kerswell, R. R. & Gilbert, A. D. 2001 Bounds on dissipation for Navier–Stokes flow with Kolmogorov forcing. *Physica* D **158** (1–4), 105–128.

Dascaliuc, R., Foias, C. & Jolly, M. S. 2009 On the asymptotic behavior of average energy and enstrophy in 3D turbulent flows. *Physica* D **238**, 725–736.

Doering, C. R. & Constantin, P. 1992 Energy dissipation in shear driven turbulence. *Phys. Rev. Lett.* **69** (11), 1648–1651.

Doering, C. R. & Constantin, P. 1994 Variational bounds on energy dissipation in incompressible flows: shear flow. *Phys. Rev.* E **49** (5), 4087–4099.

Doering, C. R., Eckhardt, B. & Schumacher, J. 2003 Energy dissipation in body-forced plane shear flow. *J. Fluid Mech.* **494**, 275–284.

Doering, C. R. & Foias, C. 2002 Energy dissipation in body-forced turbulence. *J. Fluid Mech.* **467**, 289–306.

Foias, C. 1997 What do the Navier–Stokes equations tell us about turbulence? *Contemp. Maths* **208**, 151–180.

Foias, C., Manley, O. P. & Temam, R. 1993 Bounds for the mean dissipation of the 2D enstrophy and 3D energy in turbulent flows. *Phys. Lett.* A **174**, 210–215.

Frisch, U. 1995 *Turbulence: The Legacy of A. N. Kolmogorov*. Cambridge University Press.

Howard, L. N. 1972 Bounds on flow quantities. *Annu. Rev. Fluid Mech.* **4**, 473–494.

Kerswell, R. R. 1998 Unification of variational principles for turbulent shear flows: the background method of Doering–Constantin and the mean-fluctuation formulation of Howard–Busse. *Physica* D **121** (1–2), 175–192.

Kolmogorov, A. 1941 The local structure of turbulence in incompressible viscous fluid for very large Reynolds numbers. *Dokl. Akad. Nauk SSSR* **30**, 301–305.

Petrov, N. P., Lu, L. & Doering, C. R. 2005 Variational bounds on the energy dissipation rate in body-forced shear flow. *J. Turbul.* **6**, Art. No. 17, doi:10.1080/14685240500228262.

Richardson, L. F. 1922 *Weather Prediction by Numerical Process*. Cambridge University Press.

Sarris, I. E., Jeanmart, H., Carati, D. & Winckelmans, G. 2007 Box-size dependence and breaking of translational invariance in the velocity statistics computed from three-dimensional turbulent Kolmogorov flows. *Phys. Fluids* **19**, 095101.

Sreenivasan, K. R. 1984 On the scaling of the turbulence energy dissipation rate. *Phys. Fluids* **27**, 1048–1051.

Sreenivasan, K. R. 1998 An update on the energy dissipation rate in isotropic turbulence. *Phys. Fluids* **10**, 528–529.

Taylor, G. I. 1938 The spectrum of turbulence. *Proc. R. Soc. Lond.* A **164** (919), 476–490.

Wang, X. 1997 Time-averaged energy dissipation rate for shear driven flows in $R^n$. *Physica* D **99** (4), 555–563.